Analytica Chimica Acta 1149 (2021) 238191

Contents lists available at ScienceDirect

Analytica Chimica Acta

journal homepage: www.elsevier.com/locate/aca

Impact of the size effect on enzymatic electrochemical detection based on metal-organic frameworks

Yi Feng [a], Yuting Zhao [c, *], Jun Ge [a, b, c, *]

[a] Key Laboratory of Industrial Biocatalysis, Ministry of Education, Department of Chemical Engineering, Tsinghua University, Beijing, 100084, China
[b] Institute of Biopharmaceutical and Health Engineering, Tsinghua Shenzhen International Graduate School, Shenzhen, 518055, China
[c] Institute of Biomedical Health Technology and Engineering, Shenzhen Bay Laboratory, Shenzhen, 518107, China

HIGHLIGHTS

- Cyt *c*@ZIF-8 samples with different sizes and morphologies were prepared via a one-step facile co-precipitation method.
- Cyt *c*@ZIF-8 of decreased size generated an increase in substrate affinity with a 50% decrease in the Michaelis constant K_m.
- The improved Cyt *c*@ZIF-8 presented a 6.26-fold enhancement in the enzymatic electrochemical detection sensitivity of H_2O_2.

GRAPHICAL ABSTRACT

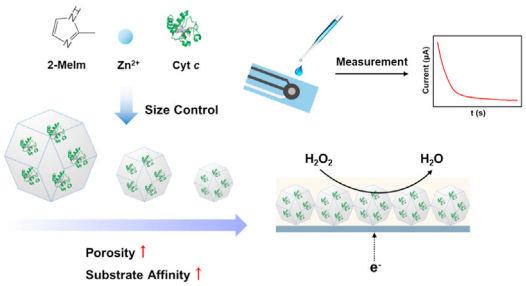

ARTICLE INFO

Article history:
Received 8 December 2020
Received in revised form
29 December 2020
Accepted 30 December 2020
Available online 4 January 2021

Keywords:
Metal-organic frameworks
Enzyme
Immobilization
Electrochemistry
Biosensor

ABSTRACT

Metal-organic frameworks (MOFs) hold a great promise as immobilization carriers for enzymes and other biomolecules, owing to their enhanced stability, selectivity and controllability. However, enzyme-MOF complexes usually lead to a decrease in the apparent enzyme activity and apparent substrate affinity as a result of the constrained structure of the enzyme and the mass transfer limitation of the substrate, respectively. These results consequently impede the applications of enzyme-MOF complexes in biocatalysis and biosensing. In this study, zeolitic imidazolate framework-8 (ZIF-8) was synthesized to immobilize cytochrome *c* (Cyt *c*) via a one-step co-precipitation process under mild conditions. By adjusting the molar ratio of precursors, enzyme-MOF composites with different sizes from 100 nm to 1.3 μm were prepared. The decreased size of the prepared MOFs generated an increase in substrate affinity (with an over 50% decrease in the Michaelis constant K_m) and a 6.4-fold improvement in the apparent enzyme activity with a 6.26-fold increase in the enzymatic electrochemical detection sensitivity compared with native Cyt *c*. The enzyme-MOF composites were coated on a screen-printed electrode for the sensitive and fast detection of H_2O_2, which is the most common representative of reactive oxygen species in cellular environments, showing the potential for the construction of efficient biosensors with applications in biomedicine.

* Corresponding authors. Institute of Biomedical Health Technology and Engineering, Shenzhen Bay Laboratory, Shenzhen, 518107, China
E-mail addresses: zhaoyt@szbl.ac.cn (Y. Zhao), junge@mail.tsinghua.edu.cn (J. Ge).

https://doi.org/10.1016/j.aca.2020.12.066
0003-2670/

1. Introduction

Metal-organic frameworks (MOFs), a broad class of excellent porous hybrid nanomaterials assembled with metal ions or clusters and organic ligands [1], have exhibited high promise for application in various fields, including gas storage, catalysis, separation, drug delivery and biosensing [2–5]. Due to their high porosity, enhanced stability, structural controllability and biocompatibility, MOFs possess potential advantages for biological applications with biomacromolecules, such as DNA, RNA and enzymes [6–8]. In recent years, MOFs with specific functional sites and biomacromolecules have been increasingly studied for the application in biosensors. For instance, Zhang and Yan reported a novel lanthanide functionalized MOF enzyme composite that could be utilized for urine fluorescence detection as a point-of care detector [9]. Muppidathi et al. reported a single-strand DNA-MOF composite for the efficient and specific recognition of harmful arsenate ions with a fluorescence quenching method [10].

The biosensors combined of enzymes and MOFs have been widely studied, which have expanded the *ex vivo* applications of enzyme in multifarious process [11,12]. To date, most studies related to enzyme-MOF biosensors have focused on employing fluorescence or chemiluminescence as the response signal, with limited examples in electrochemical detection [13,14] because of the poor conductivity, low electron transfer efficiency and low apparent enzyme activity of enzyme-MOF composites. To enhance the detection sensitivity of enzyme-MOF electrochemical biosensors, most researchers have been devoted to improving the electronic conductivity of MOF materials or increasing the electron transfer efficiency between the enzyme and electrode by doping guest molecules [3,15]. Nevertheless, less attention has been paid to increasing the apparent enzyme activity and the substrate affinity of the enzyme-MOF composite, which could be another strategy to enhance the detection performance.

In general, two methods are used to immobilize enzymes on MOFs. One is synthesizing MOFs and then absorbing enzyme molecules [16–18], the other is the one-pot co-precipitation method which can encapsulate enzyme molecules directly in one step during the formation of MOFs [19,20]. Both strategies can improve the stability of enzyme efficiently due to the rigid structure of MOFs, but the immobilization carriers also impose restrictions on substrate mass transfer, leading to a decrease in the apparent enzyme activity and substrate affinity [16,19,20]. Ge and co-workers introduced polystyrene (PS) nanospheres during the synthesis of MOFs to generate mesopores, which could be one way to facilitate the substrate mass transfer [14].

In this study, we proposed an alternative method to improve the apparent enzyme activity and substrate affinity of enzyme-MOF composites. We immobilized cytochrome *c* (Cyt *c*), which is a low-cost protein possessing the properties of peroxidase, in zeolitic imidazolate framework-8 (ZIF-8) under mild conditions through a one-step co-precipitation process. ZIF-8 is a representative MOF constructed with zinc ions and imidazolates, which is suggested to be capable of increasing the thermal and chemical stabilities of enzymes [21,22]. We explored the size effect under different conditions and utilized the structural controllability of MOFs to adjust the morphology of the nanoparticles, in order to improve the performance of the enzyme-MOF composites for electrochemical detection. Additionally, ZIF-8 possesses intrinsic biodegradability and good biocompatibility [23,24], making it a promising material for use in biosensors. The prepared Cyt *c*@ZIF-8 composite can be employed for the fast electrochemical detection of H_2O_2, which is the most common representative of reactive oxygen species (ROS), regulating various metabolic processes of humans and other organisms, including protein synthesis, cell apoptosis, and DNA damage [25,26]. Excessive amount of H_2O_2 accumulation in organisms may cause pathological events, such as autoimmune diseases, neurodegeneration and cancer [27]. Therefore, the fast and accurate determination of H_2O_2 with high sensitivity is of vital importance and has perspectives to be applied in multifarious fields, including food monitoring, pharmaceutical monitoring, clinical diagnosis and environmental analysis [28].

2. Materials and methods

2.1. Materials

2-methylimidazole (2-Melm) and 2,2′-azino-bis (3-ethylbenzothiazoline-6-sulfonic acid) diammonium salt (ABTS) were purchased from Sigma-Aldrich. Cytchrome *c* (Cyt *c*) from bovine heart was purchased from Biotopped. Zinc nitrate hexahydrate (99.998%) was purchased from Alfa Aesar. Bovine serum albumin was purchased from Solarbio. Hydrogen peroxide was purchased from Xilong Scientific Co., Ltd. The screen-printed electrode was composed of polyethylene terephthalate in 1 cm × 3 cm, the working electrode as well as the counter electrode were carbon electrodes and the reference electrode was a Ag/AgCl electrode. Other reagents were of analytical grade.

2.2. Synthesis of Cyt c@ZIF-8

Typically, 250 mM of zinc nitrate hexahydrate in 10 mL of deionized water and 781.25 mM 2-methylimidazole in 8 mL of deionized water were prepared respectively and subjected to ultrasonic treatment for 15 min. Cytochrome *c* (Cyt *c*) was dissolved in deionized water at a concentration of 10 mg/mL. The synthesis of the Cyt *c*@ZIF-$8_{1:25}$ composite was performed by mixing 2-methylimidazole solution (1.6 mL, 781.25 mM), zinc nitrate solution (0.2 mL, 250 mM) and Cyt *c* solution (50 μL, 10 mg/mL) and stirring them at room temperature for 30 min. Then, the product after the reaction was collected by centrifuging at 12,000 rpm for 5 min and washing with deionized water for 3 times. To further investigate the size effect of the Cyt *c*@ZIF-8 composites on the apparent enzyme activity and effective electrochemical detection, the composites of Cyt *c*@ZIF-$8_{1:50}$ and Cyt *c*@ZIF-$8_{1:75}$ were synthesized by adjusting the molar ratio of 2-Melm/Zn to 50 and 75 respectively.

2.3. Scanning electron microscopy (SEM) and transmission electron microscopy (TEM) analysis

The morphology of the samples was characterized by SEM (JSM7401; Japan) and TEM (JEM2010; Japan). Samples after lyophilization were coated on the conducting resin with an accelerating voltage of 3 kV for SEM. For TEM, the samples were prepared by suspending the composites in deionized water and adding a well-dispersed droplet on a carbon support film. After drying at room temperature for 24 h, the samples were observed under a JEM-2010 high-resolution TEM with an accelerating voltage of 120 kV.

2.4. Powder X-ray diffraction (XRD)

The powder X-ray diffraction (XRD) analysis was measured on a Bruker D8 Advance X-Ray diffractometer with a Cu Kα line ($\lambda = 0.15406$ nm) at 40 kV and 40 mA. XRD patterns were collected with the scanning speed of 2°/min and the diffraction angle range of 5–50°.

2.5. Thermal gravimetric analysis (TGA)

Thermal gravimetric Analysis (TGA) was performed on a TA Instruments TGA 2050 Thermogravimetric Analyzer. The sample was heated in air atmosphere from room temperature to 700 °C at the rate of 10 °C/min.

2.6. Enzymatic activity assay of Cyt c@ZIF-8

In a typical experiment, 900 μL of ABTS aqueous solution (2.74 mg/mL), 50 μL of hydrogen peroxide (0.3%) in 200 mM phosphate buffered saline solution (pH 7.4) and 20 μL of Cyt *c*@ZIF-8 suspension were well mixed in a quartz cuvette, followed by monitoring the increase in absorbance at 415 nm for 15 s in an ultraviolet spectrophotometer. The same protocol was applied to determine the enzymatic activity of free Cyt *c* at the same protein concentration.

2.7. Preparation of the Cyt c@ZIF-8 on the screen-printed electrode (SPE)

10 μL of ABTS aqueous solution (2.74 mg/mL) was dropped on the working electrode of the SPE and dried at 40 °C for 20 min, followed by dropping 10 μL of Cyt *c*@ZIF-8 suspension solution (1 mg/mL) on the working electrode and drying at 40 °C for 20 min. At last, 2 μL of Nafion (1%) as a protective layer was coated on the working electrode and dried at room temperature.

2.8. Electrochemical detection

The electrochemical experiments were performed on a Reference 600+ electrochemical workstation (Gamry, America). A typical cyclic voltammogram (CV) curve was measured with a voltage sweep range of −0.1 V–0.7 V and a scan rate of 0.1 V/s. Besides, the typical chronoamperometric response was recorded at a constant potential of 0.2 V within 100s. 100 μL of H_2O_2 in phosphate buffer saline (PBS) solution (0.1 M, pH 7.4) was applied on the prepared SPE to immerse all the three electrodes before each round of detection.

3. Results and discussion

Our strategy to synthesize the Cyt *c*@ZIF-8 composites was a one-pot co-precipitation method in aqueous phase. By adjusting the molar ratio of the MOF precursors, that is, the molar ratio of Zn/2-Melm, Cyt *c*@ZIF-8 composites with micro-to nanoscale sizes were obtained. The molar ratios of Zn/Melm were set as 1:25, 1:50 and 1:75 respectively, which are labelled at the bottom right of Cyt *c*@ZIF-8. With the molar ratio of 2-Melm/Zn higher than 75, the structure of Cyt *c*@ZIF-8 will be less robust and hard to collect. Scanning electron microscopy (SEM) images and transmission electron microscopy (TEM) images exhibited the morphologies of the Cyt *c*@ZIF-8 composites at different molar ratios of Zn/Melm (Fig. 1). Nano Measurer 1.2 software was employed to calculate the size distributions of the different Cyt *c*@ZIF-8 nanoparticles, the results of which were inset in each SEM image. The mean size of Cyt *c*@ZIF-$8_{1:25}$ was around 1.3 μm; the surface was rough and relatively irregular with a relatively low level of crystallinity (Fig. 1a and d). With the increase in the 2-Melm/Zn molar ratio, the size of the Cyt *c*@ZIF-8 composites decreased conspicuously. The average sizes of the Cyt *c*@ZIF-$8_{1:50}$ and Cyt *c*@ZIF-$8_{1:75}$ nanoparticles were around 240 nm and 110 nm respectively, with more uniform and regular shapes and surfaces (Fig. 1b, c, 1e and 1f). The SEM images of pure ZIF-8 at different Zn/Melm molar ratios revealed that the addition of Cyt *c* had little impact on the morphology of the MOF nanoparticles (Figs. S1–S3).

The Cyt *c*@ZIF-$8_{1:25}$, Cyt *c*@ZIF-$8_{1:50}$ and Cyt *c*@ZIF-$8_{1:75}$ composites presented similar X-ray diffraction (XRD) patterns compared with simulated ZIF-8 pattern, demonstrating the well-preserved polymorph of the Cyt *c*@ZIF-8 composites when embedding protein and adjusting the molar ratio of Zn/Melm (Fig. 2a). Moreover, the XRD pattern of Cyt *c*@ZIF-$8_{1:25}$ exhibited the decreased crystallinity when 2-Melm/Zn was relatively low, which corresponded with the SEM images, demonstrating that regulating the molar ratio of metal ions and organic ligands can adjust and control the crystallinity of MOFs. Thermal gravimetric analysis (TGA) in air confirmed around 10 wt% of protein was immobilized in the Cyt *c*@ZIF-8 composites (Fig. 2b, Figs. S4 and S5).

To explore the effect of different size distributions of ZIF-8, the Brunner–Emmet–Teller (BET) characterization method was taken. The nitrogen adsorption curves and DFT pore size distributions are shown in Fig. 2c and d. The corresponding specific surface areas and pore volumes of ZIF-$8_{1:25}$, ZIF-$8_{1:50}$ and ZIF-$8_{1:75}$ are displayed in Table 1. As the size of ZIF-8 decreased by adjusting the molar ratio of Zn/Melm, the specific surface area of ZIF-8 increased conspicuously, which provided more surface area for the interaction between substrates and enzymes immobilized in ZIF-8. Additionally, the pore volume of ZIF-$8_{1:75}$ was 1.6-fold higher than that of ZIF-$8_{1:50}$ and 4.4-fold higher than that of ZIF-$8_{1:25}$. The enhanced pore volume was conducive to improving the efficiency of the immobilization of bio-macromolecules in MOFs.

The enzymatic activities of Cyt *c*@ZIF-8 composites and native Cyt *c* were measured by referring to a standard method [29] with hydrogen peroxide (H_2O_2) (0.3%) as the oxide substrate and 2,2′-azinobis (3-ethylbenzthiazoline-6-sulfonate) (ABTS) (2.74 mg/mL) as the chromogenic substrate in phosphate buffered saline solution (200 mM, pH 7.4). The encapsulation efficiency of Cyt *c* in the co-precipitation process was calculated as around 60% utilizing a Bradford assay kit. As shown in Fig. 3a, compared with native Cyt *c*, the enzymatic activities of the Cyt *c*@ZIF-8 composites were enhanced significantly. Meanwhile, the relative activities of the Cyt *c*@ZIF-8 composites were improved with the increase in the 2-Melm molar ratio, that is, the decrease in the particle size, from a 4.3-fold increase to a 6.4-fold increase compared with native Cyt *c*, demonstrating the successful regulation of enzymatic catalytic efficiency by utilizing structural controllability. In addition, the apparent Michaelis constant K_m decreased by over 50% as the size of the composites decreased, from 489 mM of Cyt *c*@ZIF-$8_{1:25}$–234 mM of Cyt *c*@ZIF-$8_{1:75}$ (Figs. S6–S8). The apparent Michaelis constant represented the affinity between the substrates and enzyme-MOF composites, the decrease of which indicated the increase in substrate affinity. It was proven that the reduction in composite size could provide an increase in the specific surface area and porosity of enzyme-MOF nanoparticles, generating a significant improvement in substrate affinity, thereby providing another way to improve the performance of enzyme-MOF composites.

During the immobilization or encapsulation process of protein, a loss of enzymatic activity often occurs, which is mainly caused by the increased mass transfer resistance and the change in protein conformation related to the microenvironment of the active site within the immobilization carriers [20]. In this study, the mechanism behind the significant enzymatic activity increase of Cyt *c*@ZIF-8 composites needs to be explored. The active site of Cyt *c* is mainly derived from the heme group. Native Cyt *c* exhibits a six-coordinate low spin state with two axial ligands in the Fe center, leading to a compact structure which is difficult for enzyme-substrate reactions [30]. When Cyt *c* is embedded in MOFs, the microenvironment around the active site changes, generating partial protein unfolding and exposing the heme groups. Utilizing solid-state UV–Vis, paramagnetic resonance spectroscopy and

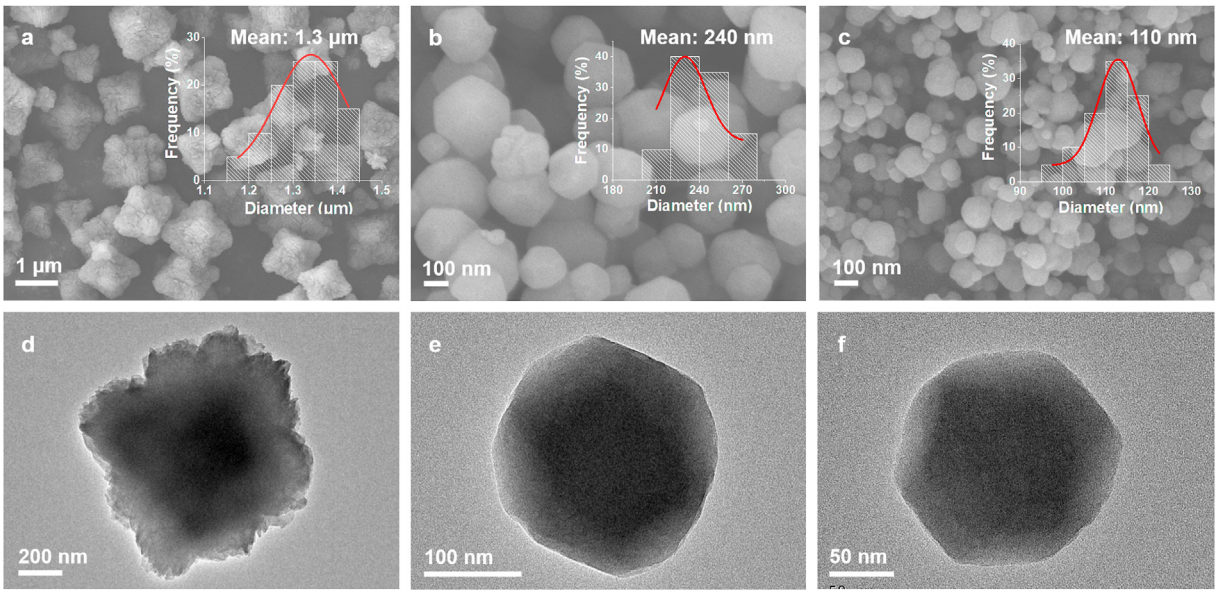

Fig. 1. SEM images of (a) Cyt *c*@ZIF-$8_{1:25}$, (b) Cyt *c*@ZIF-$8_{1:50}$ and (c) Cyt *c*@ZIF-$8_{1:75}$. The size distributions of different Cyt *c*@ZIF-8 nanoparticles were calculated with Nano Measurer 1.2 and inset in each SEM image. TEM images of (d) Cyt *c*@ZIF-$8_{1:25}$, (e) Cyt *c*@ZIF-$8_{1:50}$ and (f) Cyt *c*@ZIF-$8_{1:75}$.

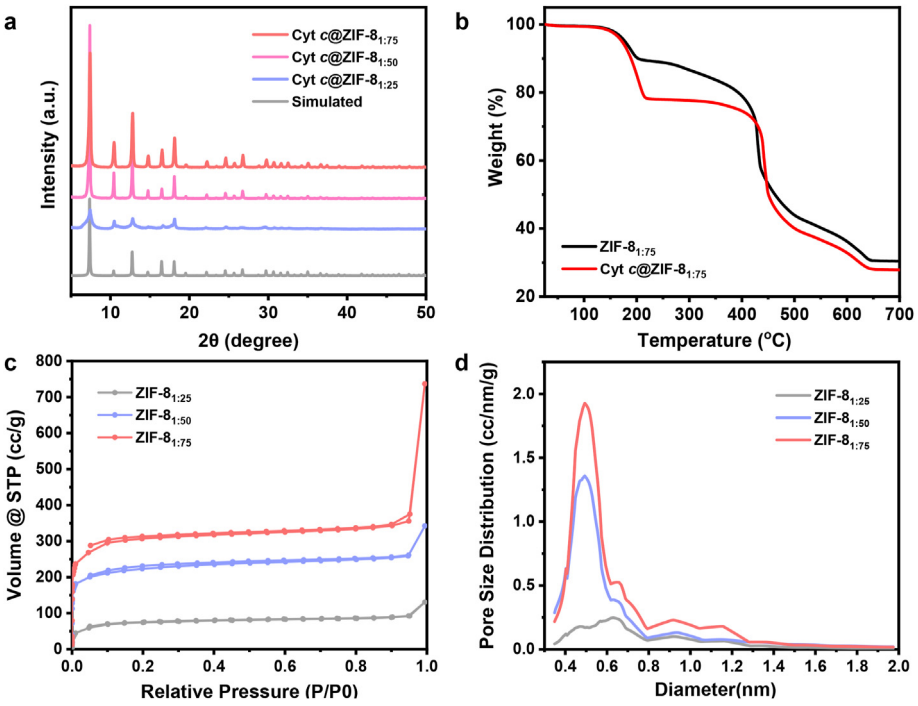

Fig. 2. (a) XRD patterns of simulated ZIF-8 (black), Cyt *c*@ZIF-$8_{1:25}$ (blue), Cyt *c*@ZIF-$8_{1:50}$ (pink) and Cyt *c*@ZIF-$8_{1:75}$ (red). (b) TGA curves of Cyt *c*@ZIF-$8_{1:75}$ and pure ZIF-$8_{1:75}$ in air. (c) Nitrogen adsorption curves of ZIF-$8_{1:25}$ (black), ZIF-$8_{1:50}$ (blue) and ZIF-$8_{1:75}$ (red). (d) DFT pore size distributions of ZIF-$8_{1:25}$ (black), ZIF-$8_{1:50}$ (blue) and ZIF-$8_{1:75}$ (red). (For interpretation of the references to colour in this figure legend, the reader is referred to the Web version of this article.)

Table 1
The specific surface area and pore volume of ZIF-$8_{1:25}$, ZIF-$8_{1:50}$ and ZIF-$8_{1:75}$.

Samples	Specific Surface Area (m^2/g)	Pore Volume (cm^3/g)
ZIF-$8_{1:25}$	262	0.145
ZIF-$8_{1:50}$	844	0.297
ZIF-$8_{1:75}$	1141	0.784

molecular dynamics simulation, Chen et al. recently discovered that when Cyt *c* is encapsulated, the structure around its active center changes with a loss of low spin heme species and a perturbation of the iron coordination environment, leading to increased accessibility between reaction substrates and Cyt *c* active center [31]. Furthermore, as the particle size of the Cyt *c*@ZIF-8 composite decreased from micro-to nanoscale, the specific surface area and porosity of the composite increased significantly, leading to easier contact between the substrate and Cyt *c* active site, which

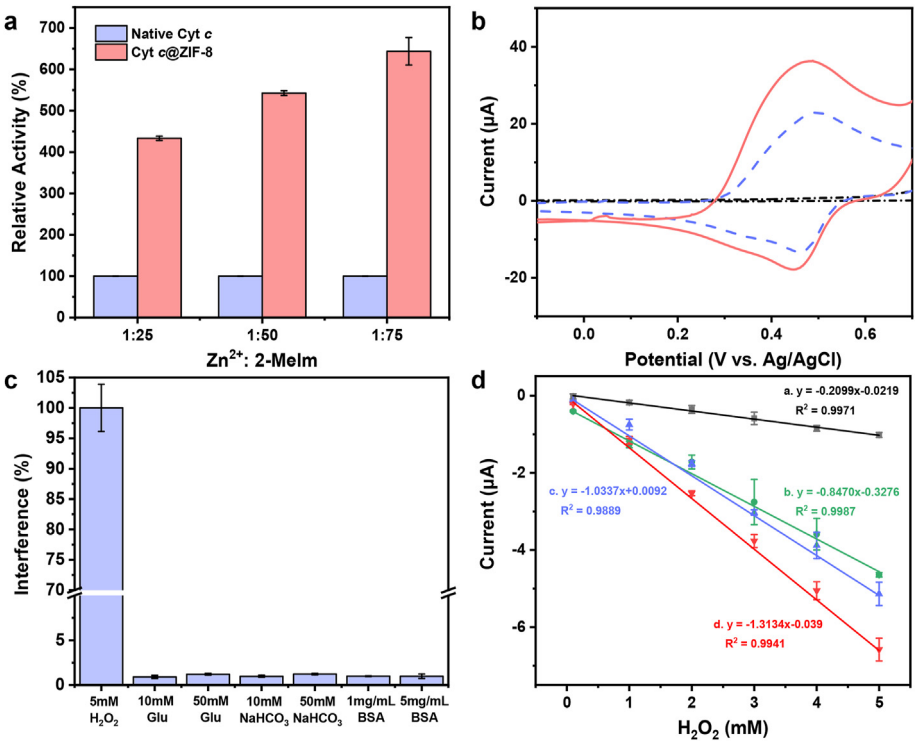

Fig. 3. (a) Relative activities of Cyt *c*@ZIF-$8_{1:25}$, Cyt *c*@ZIF-$8_{1:50}$ and Cyt *c*@ZIF-$8_{1:75}$ composites compared with native Cyt *c*. (b) Cyclic voltammograms for Cyt *c*@ZIF-8/SPE in PBS buffer without ABTS (black), in PBS buffer with ABTS (blue), in PBS buffer containing 10 mM H_2O_2 with ABTS (red). (c) Interference experiment results of Cyt *c*@ZIF-$8_{1:75}$/SPE with amperometric response of different analytes, including H_2O_2, glucose (Glu), $NaHCO_3$ and BSA. (d) Concentration curve of the chronoamperometric response at 40 s against different H_2O_2 concentrations for Cyt *c*/SPE (black), Cyt *c*@ZIF-$8_{1:25}$/SPE (green), Cyt *c*@ZIF-$8_{1:50}$/SPE (blue) and Cyt *c*@ZIF-$8_{1:75}$/SPE (red). (For interpretation of the references to colour in this figure legend, the reader is referred to the Web version of this article.)

presented a further increase in the apparent enzyme activity and substrate affinity.

The Cyt *c*@ZIF-8 composites with improved apparent enzyme activity and substrate affinity were employed for the fast electrochemical detection of H_2O_2, the most common representative of ROS. The determination process was realized through a portable screen-printed electrode (SPE) and Gamry Reference 600+ electrochemical workstation. Cyclic voltammetry (CV) studies were implemented to examine the redox behavior of the Cyt *c*@ZIF-8/SPE electrode. Typical CV curves were obtained at a scan rate of 0.1 V/s by adding 100 μL of phosphate buffered saline (PBS) solution (with and without H_2O_2) to the SPE, immersing all the three electrodes. ABTS served as the micromolecular electron mediator in the electron transfer process. As depicted in Fig. 3b, the CV curve of Cyt *c*@ZIF-8/SPE without ABTS in pure PBS presented no redox peak and weak current, revealing a poor electron transfer efficiency between Cyt *c* and the electrode. The Cyt *c*@ZIF-8/SPE with ABTS exhibited a couple of obvious redox peaks, indicating the effective electron transfer among the substrate, Cyt *c* and the electrode with the assistance of ABTS. The cathodic peak potential (E_{pc}) and anodic peak potential (E_{pa}) were located at 0.46 V and 0.50 V (vs. Ag/AgCl) respectively, with a peak-to-peak separation (ΔE_p) of 40 mV. With ABTS served as the electron mediator, the principle of catalyzing H_2O_2 could be described using the following equation.

$$\text{Cyt } c\text{-Fe(III)} + e^- \rightarrow \text{Cyt } c\text{-Fe(II)} \quad (1)$$

$$2\text{Cyt } c\text{-Fe(II)} + H_2O_2 + 2H^+ \rightarrow 2\text{Cyt } c\text{-Fe(III)} + 2H_2O \quad (2)$$

From the electrochemical mechanism equation, it was indicated that the cathodic peak of the cyclic voltammetry curve reflected the reduction of Cyt *c* that was oxidized by H_2O_2 molecules in solution.

The chronoamperometric experiment was carried out to determine the electrocatalytic response of the Cyt *c*@ZIF-8/SPE towards H_2O_2 at different concentrations. The amperometric current responses of Cyt *c*, Cyt *c*@ZIF-$8_{1:25}$/SPE, Cyt *c*@ZIF-$8_{1:50}$/SPE and Cyt *c*@ZIF-$8_{1:75}$/SPE were detected respectively. The amperometric current response curves showed that the current values reached a steady state rapidly, which had potential to conveniently achieve quick electrochemical detection (Figs. S9–S12). As the increase of H_2O_2 concentration, it took a slightly longer time for the current signal to be stable. Finally, the current value at 40 s was selected to plot the calibration curve graph. It was revealed that the four kinds of electrodes presented a linear response from ~0.1 to ~5 mM H_2O_2 (Fig. 3d). The detection sensitivity, that is the slope of the H_2O_2 concentration curve, of Cyt *c*@ZIF-81:75/SPE showed a 1.55-fold increase compared with that of Cyt *c*@ZIF-$8_{1:25}$/SPE and an approximately 1.27-fold increase compared with that of Cyt *c*@ZIF-$8_{1:50}$/SPE (Fig. 3d). Moreover, compared with native Cyt *c*/SPE, the detection sensitivities of Cyt *c*@ZIF-8/SPEs were enhanced from 4.04 fold of Cyt *c*@ZIF-81:25/SPE to 6.26 fold of Cyt *c*@ZIF-81:75/SPE (Fig. 3d). The amounts of protein were consistent between native Cyt *c* and Cyt *c*@ZIF-8 on the SPE. The performance of ZIF-8 modified enzymatic electrode was improved due to the enhanced enzymatic activity of immobilized Cyt *c*@ZIF-8 instead of the intrinsic catalytic activity of pure ZIF-8. As shown in Figs. S13–S15, the amperometric current response remained close to zero as the increase of H_2O_2 concentration on ZIF-8/SPE, demonstrating that no catalytic events occurred with pure ZIF-8 on the SPE. In addition to the improvement of enzymatic activities, this porous immobilization material may play a vital role in gathering the substrates, which could be another way of increasing the property of the enzymatic electrode. The experimental results indicated that the

increased sensitivity of enzymatic reaction could be realized by regulating the structure and size of MOF particles, which generated the enhancement of substrate affinity and apparent enzymatic activity, as demonstrated before. This result also verified our previous hypothesis that the detection performance of enzyme electrodes could be improved by increasing the apparent enzyme activity and substrate affinity, which was achieved by utilizing the structural controllability of MOFs. The interference experiment was conducted to prove the high selectivity of Cyt *c*@ZIF-$8_{1:75}$/SPE. As shown in Fig. 3c, the amperometric response of H_2O_2 was much higher than that of other interferences, including glucose, $NaHCO_3$ and BSA, although these interferences are at much higher concentration, that is, 2-fold−10-fold concentrations. The results above demonstrated that Cyt *c*@ZIF-$8_{1:75}$/SPE had both excellent sensitivity and selectivity.

This study provided a novel strategy to improve the detection sensitivity of enzymatic electrodes, that is to enhance the substrate affinity except for increasing the electron transfer efficiency. In most cases, immobilized enzymes as sensitive elements presented increased stability while displaying decreased apparent substrate affinity due to the restricted mass-diffusion rate of substrates [14,32,33], which meant the substrates were exhausted before accumulating. This work took full advantage of the structure controllability of MOFs to increase the porosity of the immobilization carriers by conveniently adjusting the molar ratio of metal ions and organic ligands, leading to lower mass transfer resistance and generating improved apparent substrate affinity. This improved Cyt *c*@ZIF-$8_{1:75}$/SPE shows application potential for the fast detection of H_2O_2 and other ROS in food industry, environmental analysis or medical detection fields.

4. Conclusion

In conclusion, a series of Cyt *c*@ZIF-8 composites with different sizes and morphologies were synthesized. The mechanism of the size effect was investigated in depth. By utilizing the structural controllability and size effect of MOFs, the specific surface area and the porosity of the enzyme immobilization carrier were increased significantly, generating a 50% decrease in the Michaelis constant K_m and a 6.4-fold increase in the apparent enzymatic activity. Cyt *c*@ZIF-$8_{1:75}$/SPE presented a 1.55-fold increase compared to Cyt *c*@ZIF-$8_{1:25}$/SPE and 6.26-fold increase compared to Cyt *c*/SPE in the detection sensitivity of H_2O_2, meanwhile excellent specificity remained. The size-optimized composite exhibited its potential application perspectives in the construction of efficient biosensors for the fast detection of H_2O_2 and other ROS in environmental analysis, food industry and medical detection.

CRediT authorship contribution statement

Yi Feng: Conceptualization, Methodology, Software, Data curation, Visualization, Investigation, Writing - original draft, preparation. **Yuting Zhao:** Writing - review & editing. **Jun Ge:** Supervision, Funding acquisition.

Declaration of competing interest

The authors declare that they have no known competing financial interests or personal relationships that could have appeared to influence the work reported in this paper.

Acknowledgement

This work was supported by the National Natural Science Foundation of China (21911540467, 21878174).

Appendix A. Supplementary data

Supplementary data to this article can be found online at https://doi.org/10.1016/j.aca.2020.12.066.

References

[1] H. Li, M. Eddaoudi, M. O'Keeffe, O.M. Yaghi, Design and synthesis of an exceptionally stable and highly porous metal-organic framework, Nature 402 (6759) (1999) 276−279.
[2] Y. Cui, B. Li, H. He, W. Zhou, B. Chen, G. Qian, Metal-organic frameworks as platforms for functional materials, Accounts Chem. Res. 49 (3) (2016) 483−493.
[3] G. Li, S. Zhao, Y. Zhang, Z. Tang, Metal-organic frameworks encapsulating active nanoparticles as emerging composites for catalysis: recent progress and perspectives, Adv. Mater. 30 (51) (2018).
[4] L. Wang, M. Zheng, Z. Xie, Nanoscale metal-organic frameworks for drug delivery: a conventional platform with new promise, J. Math. Chem. B 6 (5) (2018) 707−717.
[5] J. Zhou, G. Tian, L. Zeng, X. Song, X.-w. Bian, Nanoscaled metal-organic frameworks for biosensing, imaging, and cancer therapy, Adv. Healthc. Mater. 7 (10) (2018).
[6] K. Liang, R. Ricco, C.M. Doherty, M.J. Styles, S. Bell, N. Kirby, S. Mudie, D. Haylock, A.J. Hill, C.J. Doonan, P. Falcaro, Biomimetic mineralization of metal-organic frameworks as protective coatings for biomacromolecules, Nat. Commun. 6 (2015).
[7] S.K. Alsaiari, S. Patil, M. Alyami, K.O. Alamoudi, F.A. Aleisa, J.S. Merzaban, M. Li, N.M. Khashab, Endosomal escape and delivery of CRISPR/Cas9 genome editing machinery enabled by nanoscale zeolitic imidazolate framework, J. Am. Chem. Soc. 140 (1) (2018) 143−146.
[8] X. Wu, M. Hou, J. Ge, Metal-organic frameworks and inorganic nanoflowers: a type of emerging inorganic crystal nanocarrier for enzyme immobilization, Catal. Sci. Technol. 5 (12) (2015) 5077−5085.
[9] Y. Zhang, B. Yan, A point-of-care diagnostics logic detector based on glucose oxidase immobilized lanthanide functionalized metal-organic frameworks, Nanoscale 11 (47) (2019) 22946−22953.
[10] M. Muppidathi, P. Perumal, R. Ayyanu, S. Subramanian, Immobilization of ssDNA on a metal-organic framework derived magnetic porous carbon (MPC) composite as a fluorescent sensing platform for the detection of arsenate ions, Analyst 144 (9) (2019) 3111−3118.
[11] X. Lian, Y. Fang, E. Joseph, Q. Wang, J. Li, S. Banerjee, C. Lollar, X. Wang, H.-C. Zhou, Enzyme-MOF (metal-organic framework) composites, Chem. Soc. Rev. 46 (11) (2017) 3386−3401.
[12] W. Duan, Z. Zhao, H. An, Z. Zhang, P. Cheng, Y. Chen, H. Huang, State-of-the-Art and prospects of biomolecules: incorporation in functional metal-organic frameworks, Top. Curr. Chem. 377 (6) (2019).
[13] X. Liao, H. Fu, T. Yan, J. Lei, Electroactive metal-organic framework composites: design and biosensing application, Biosens. Bioelectron. 146 (2019).
[14] C. Zhang, X. Wang, M. Hou, X. Li, X. Wu, J. Ge, Immobilization on metal-organic framework engenders high sensitivity for enzymatic electrochemical detection, ACS Appl. Mater. Interfaces 9 (16) (2017) 13831−13836.
[15] T.-Z. Liu, R. Hu, X. Zhang, K.-L. Zhang, Y. Liu, X.-B. Zhang, R.-Y. Bai, D. Li, Y.-H. Yang, Metal-organic framework nanomaterials as novel signal probes for electron transfer mediated ultrasensitive electrochemical immunoassay, Anal. Chem. 88 (24) (2016) 12516−12523.
[16] V. Lykourinou, Y. Chen, X.-S. Wang, L. Meng, H. Tran, L.-J. Ming, R.L. Musselman, S. Ma, Immobilization of MP-11 into a mesoporous metal-organic framework, MP-11@mesoMOF: a new platform for enzymatic catalysis, J. Am. Chem. Soc. 133 (27) (2011) 10382−10385.
[17] P. Li, S.-Y. Moon, M.A. Guelta, L. Lin, D.A. Gomez-Gualdron, R.Q. Snurr, S.P. Harvey, J.T. Hupp, O.K. Farha, Nanosizing a metal-organic framework enzyme carrier for accelerating nerve agent hydrolysis, ACS Nano 10 (10) (2016) 9174−9182.
[18] Y. Chen, V. Lykourinou, C. Vetromile, H. Tran, L.-J. Ming, R.W. Larsen, S. Ma, How can proteins enter the interior of a MOF? Investigation of cytochrome c translocation into a MOF consisting of mesoporous cages with microporous windows, J. Am. Chem. Soc. 134 (32) (2012) 13188−13191.
[19] F. Lyu, Y. Zhang, R.N. Zare, J. Ge, Z. Liu, One-pot synthesis of protein-embedded metal-organic frameworks with enhanced biological activities, Nano Lett. 14 (10) (2014) 5761−5765.
[20] X. Wu, J. Ge, C. Yang, M. Hou, Z. Liu, Facile synthesis of multiple enzyme-containing metal-organic frameworks in a biomolecule-friendly environment, Chem. Commun. 51 (69) (2015) 13408−13411.
[21] S. Liang, X.-L. Wu, J. Xiong, M.-H. Zong, W.-Y. Lou, Metal-organic frameworks as novel matrices for efficient enzyme immobilization: an update review, Coord. Chem. Rev. 406 (2020).
[22] Y.V. Kaneti, S. Dutta, M.S.A. Hossain, M.J.A. Shiddiky, K.-L. Tung, F.-K. Shieh, C.-K. Tsung, K.C.W. Wu, Y. Yamauchi, Strategies for improving the functionality of zeolitic imidazolate frameworks: tailoring nanoarchitectures for functional applications, Adv. Mater. 29 (38) (2017).
[23] H.-S. Wang, Metal-organic frameworks for biosensing and bioimaging applications, Coord. Chem. Rev. 349 (2017) 139−155.
[24] W. Liu, Y. Pan, W. Xiao, H. Xu, D. Liu, F. Ren, X. Peng, J. Liu, Recent

developments on zinc(II) metal-organic framework nanocarriers for physiological pH-responsive drug delivery, MedChemComm 10 (12) (2019) 2038–2051.
[25] Y. Zhang, X. Bai, X. Wang, K.-K. Shiu, Y. Zhu, H. Jiang, Highly sensitive graphene-Pt nanocomposites amperometric biosensor and its application in living cell H_2O_2 detection, Anal. Chem. 86 (19) (2014) 9459–9465.
[26] Y. Zhang, C. Wu, X. Zhou, X. Wu, Y. Yang, H. Wu, S. Guo, J. Zhang, Graphene quantum dots/gold electrode and its application in living cell H_2O_2 detection, Nanoscale 5 (5) (2013) 1816–1819.
[27] F. Pagliari, C. Mandoli, G. Forte, E. Magnani, S. Pagliari, G. Nardone, S. Licoccia, M. Minieri, P. Di Nardo, E. Traversa, Cerium oxide nanoparticles protect cardiac progenitor cells from oxidative stress, ACS Nano 6 (5) (2012) 3767–3775.
[28] F. Zhang, Z. Wang, Y. Zhang, Z. Zheng, C. Wang, Y. Du, W. Ye, Microwave-assisted synthesis of Pt/graphene nanocomposites for nonenzymatic hydrogen peroxide sensor, Int. J. Electrochem. Sci. 7 (3) (2012) 1968–1977.
[29] M. Ozgen, R.N. Reese, A.Z. Tulio, J.C. Scheerens, A.R. Miller, Modified 2,2-azino-bis-3-ethylbenzothiazoline-6-sulfonic acid (ABTS) method to measure antioxidant capacity of selected small fruits and comparison to ferric reducing antioxidant power (FRAP) and 2,2 '-diphenyl-1-picrylhydrazyl (DPPH) methods, J. Agric. Food Chem. 54 (4) (2006) 1151–1157.
[30] Z. Liu, H. Lin, S. Ye, Q.-Y. Liu, Z. Meng, C.-M. Zhang, Y. Xia, E. Margoliash, Z. Rao, X.-J. Liu, Remarkably high activities of testicular cytochrome c in destroying reactive oxygen species and in triggering apoptosis, Proc. Natl. Acad. Sci. U. S. A 103 (24) (2006) 8965–8970.
[31] Y. Chen, F. Jimenez-Angeles, B. Qiao, M.D. Krzyaniak, F. Sha, S. Kato, X. Gong, C.T. Buru, Z. Chen, X. Zhang, N.C. Gianneschi, M.R. Wasielewski, M.O. de la Cruz, O.K. Farha, Insights into the enhanced catalytic activity of cytochrome c when encapsulated in a metal-organic framework, J. Am. Chem. Soc. 142 (43) (2020) 18576–18582.
[32] X. Wu, H. Yue, Y. Zhang, X. Gao, X. Li, L. Wang, Y. Cao, M. Hou, H. An, L. Zhang, S. Li, J. Ma, H. Lin, Y. Fu, H. Gu, W. Lou, W. Wei, R.N. Zare, J. Ge, Packaging and delivering enzymes by amorphous metal-organic frameworks, Nat. Commun. 10 (2019).
[33] C. Huang, Z. Guo, X. Zheng, X. Chen, Z. Xue, S. Zhang, X. Li, B. Guan, X. Li, G. Hu, T. Wang, Deformable metal-organic framework nanosheets for heterogeneous catalytic reactions, J. Am. Chem. Soc. 142 (20) (2020) 9408–9414.